

## Model dielectric constants of Si and Ge

Sadao Adachi

*Department of Electronic Engineering, Faculty of Engineering, Gunma University, Kiryu-shi, Gunma 376, Japan*

(Received 12 August 1988)

A method is described for calculation of the real ( $\epsilon_1$ ) and imaginary parts ( $\epsilon_2$ ) of the dielectric function of Si and Ge at energies below and above the fundamental absorption edge, in which the model is based on the Kramers-Kronig transformation and strongly connected with the electronic energy-band structure of the medium. A complete set of the critical points (CP's) are considered in this study. This model reveals distinct structures at energies of the  $E_0$ ,  $E_0 + \Delta_0$  [three-dimensional (3D)  $M_0$ ],  $E_1$ ,  $E_1 + \Delta_1$  (3D  $M_1$  or 2D  $M_0$ ),  $E_2$  [a mixture of damped harmonic oscillator (DHO) and 2D  $M_2$ ],  $E'_1$ , and  $E'_0$  (triplet) CP's (DHO). The indirect-band-gap transitions also play an important part in the spectral dependence of  $\epsilon_2$  of Si. Results are in satisfactory agreement with the experimental information over the entire range of photon energies. The strength and broadening parameters at energies of each CP are obtained and discussed.

### I. INTRODUCTION

Studies of the optical properties of solids have proved to be a powerful tool in our understanding of the electronic energy-band structures of these solids.<sup>1</sup> The dielectric function,  $\epsilon(\omega) = \epsilon_1(\omega) + i\epsilon_2(\omega)$ , is known to describe the optical properties of the medium at all photon energies  $E = \hbar\omega$ . Real and imaginary parts of this dielectric function are connected by the Kramers-Kronig (KK) relations:

$$\epsilon_1(\omega) = 1 + \frac{2}{\pi} \int_0^\infty \frac{\omega' \epsilon_2(\omega')}{(\omega')^2 - \omega^2} d\omega',$$

$$\epsilon_2(\omega) = -\frac{2}{\pi} \int_0^\infty \frac{\omega' \epsilon_1(\omega')}{(\omega')^2 - \omega^2} d\omega'.$$

Spectroscopic ellipsometry is an excellent technique with which to investigate the optical response of semiconductors.<sup>2-20</sup> Recently, Aspnes and Studna<sup>4</sup> have studied optical properties of Si and Ge by spectroscopic ellipsometry. They reported room-temperature pseudodielectric-function data and related optical constants of Si and Ge for energies  $E$  from 1.5 to 6.0 eV. Vinã *et al.*<sup>7</sup> also studied the temperature dependence of the dielectric function of Ge in the temperature range between 100 and 850 K by spectroscopic ellipsometry ( $E = 1.25-5.6$  eV). They obtained broadening parameters, amplitudes, and phase angles for the  $E_1$ ,  $E_1 + \Delta_1$ ,  $E'_0$ , and  $E_2$  critical points (CP's). They also found a decrease of the excitonic interaction with increasing temperature. More recently, Lautenschlager *et al.*<sup>19</sup> measured the dielectric function of Si by ellipsometry in the (1.7-5.7)-eV photon-energy range. They obtained the parameters of the  $E'_0$ ,  $E_1$ ,  $E_2$ , and  $E'_1$  CP's at temperatures between 30 and 820 K. However, these spectral-dependence data seem to have one disadvantage with respect to theoretical modeling: they are not expressed as continuous analytic functions of the photon energies.

In this paper we present a method for calculation of

the spectral dependence of the dielectric constants,  $\epsilon_1(\omega)$  and  $\epsilon_2(\omega)$ , of Si and Ge based on a simplified model of the energy-band structures of the materials. This model covers the optical response of Si and Ge over the entire range of photon energies. In Sec. II we present a brief review of material properties of Si and Ge with particular emphasis on their electronic energy-band structures. This information will be used to build a theoretical model in the next section. We describe in Sec. III the details of our model, which is based on the KK transformation and includes the  $E_0$ ,  $E_0 + \Delta_0$ ,  $E_1$ ,  $E_1 + \Delta_1$ ,  $E_2$ ,  $E'_1$ , and  $E'_0$  (triplet) gaps as the main dispersion mechanisms. The effects of indirect-band-gap transitions, which will play an important part in the analysis of the  $\epsilon_2$  spectrum (Si), are also discussed. In Sec. IV we show the fits with our model to the experimental data of Si and Ge reported by Philipp and Ehrenreich (Ref. 21) and Aspnes and Studna (Ref. 4). Finally, in Sec. V the conclusions obtained in this study are briefly summarized.

### II. ENERGY-GAP ARGUMENT

Si and Ge have been the subject of considerable research and device-development activities. A wide variety of calculations<sup>22-56</sup> and experiments<sup>57-103</sup> have given detailed information about their electronic energy-band structures. We reproduce in Fig. 1 the energy-band structures of Si and Ge along two lines of high symmetry from the center to the boundary of the first Brillouin zone (BZ) (see, e.g., Refs. 33 and 35). The electronic states are labeled using the notation for the representations of the single group of the diamond structure.<sup>104</sup> The locations of several interband transitions are included in the figure. These are the transitions which may play an important part in the analysis of  $\epsilon_1$  and  $\epsilon_2$  spectra. We also list in Tables I and II indirect-band-gap and CP energies of the main structure present in the optical spectra of Si (Table I) and Ge (Table II) at 300 K taken from the literature reported.



TABLE II. Energies of indirect-band-gap ( $E_g^{\text{id}}$ ) and critical points in Ge at 300 K (in eV).

$E_g^{\text{id}}$	$E_0$	$E_0 + \Delta_0$	$E_1$	$E_1 + \Delta_1$	$E'_0$	$E'_0 + \Delta'_0$	$E'_0 + \Delta'_0 + \Delta_0$	$E_2$	$E'_1$
0.6657 <sup>a</sup>	0.802 <sup>b</sup>								
	0.798 <sup>c</sup>	1.09 <sup>c</sup>							
	0.80 <sup>d</sup>	1.09 <sup>d</sup>							
	0.796 <sup>e</sup>	1.092 <sup>c</sup>	2.09 <sup>e</sup>	2.26 <sup>e</sup>					
			2.12 <sup>f</sup>	2.34 <sup>f</sup>	3.13 <sup>f</sup>	3.32 <sup>f</sup>		4.42 <sup>f</sup>	
			2.065 <sup>g</sup>	2.266 <sup>g</sup>					
			2.087 <sup>g</sup>	3.291 <sup>g</sup>					
			2.09 <sup>h</sup>	2.29 <sup>h</sup>				4.35 <sup>h</sup>	
			2.105 <sup>i</sup>	2.303 <sup>i</sup>					
			2.126 <sup>i</sup>	2.332 <sup>i</sup>					
			2.107 <sup>j</sup>	2.303 <sup>j</sup>					
			2.11 <sup>k</sup>	2.31 <sup>k</sup>				4.44 <sup>k</sup>	
			2.111 <sup>l</sup>	2.298 <sup>l</sup>	3.110 <sup>l</sup>			4.368 <sup>l</sup>	
			2.115 <sup>m</sup>	2.325 <sup>m</sup>					
			2.12 <sup>n</sup>	2.32 <sup>n</sup>	2.80 <sup>n</sup>	2.93 <sup>n</sup>			
			2.15 <sup>o</sup>	2.35 <sup>o</sup>					
					2.92 <sup>p</sup>				
					2.983 <sup>q</sup>	3.169 <sup>q</sup>	3.470 <sup>q</sup>		
									5.80 <sup>r</sup>

<sup>a</sup>Reference 57.<sup>b</sup>Reference 68.<sup>c</sup>Reference 69.<sup>d</sup>Reference 70.<sup>e</sup>Reference 71.<sup>f</sup>Reference 62.<sup>g</sup>Reference 72.<sup>h</sup>Reference 73.<sup>i</sup>Reference 74.<sup>j</sup>Reference 75.<sup>k</sup>Reference 61.<sup>l</sup>Reference 7.<sup>m</sup>Reference 76.<sup>n</sup>Reference 77.<sup>o</sup>Reference 78.<sup>p</sup>Reference 79.<sup>q</sup>Reference 80.<sup>r</sup>Present work.

cise low-field electroreflectance analysis<sup>91</sup> revealed that the  $E_2$  structure consists of three CP's,  $E_2(1)$ ,  $E_2(2)$ , and  $E_2(3)$ , of type  $M_1$ ,  $M_1$ , and  $M_2$ , respectively. It was concluded that this is due to an accidental coincidence of the  $M_1$  saddle point in the  $\langle 110 \rangle$  directions ( $\Sigma_2^v \rightarrow \Sigma_3^c$ ) and an  $M_2$  saddle point near  $X$  ( $\Delta_5^v \rightarrow \Delta_1^c$ ).

The energy-band structure of Ge is essentially the same as that of Si because both materials have the same crystal structure (i.e., diamond lattice). However, the conduction-band ordering at the  $\Gamma$  point of Ge is quite different from that of Si (but is the same as those of zinc-blende, III-V materials), as mentioned above.

The Ge crystal is an indirect-band-gap semiconductor. The lowest indirect-absorption edge of Ge corresponds to transitions from the highest valence band at the  $\Gamma$  point ( $\Gamma_{25}^v$ ) to the lowest conduction band at or near  $L$  ( $L_1$  or  $\Lambda_1$ ). As in the zinc-blende materials, the lowest direct-band-gap transitions in Ge occur in the center of the BZ [ $E_0$ :  $\Gamma_{25}^v(\Gamma_8^v) \rightarrow \Gamma_2^c(\Gamma_6^c)$ ]. The  $E_1$  edge results from transitions in the  $\Lambda$  directions of the BZ. The next prominent structure,  $E_2$ , is attributed to an accidental coincidence of an  $M_1$  saddle point at  $X$  and an  $M_2$  saddle point in the  $\Sigma$  directions.<sup>30,31,39</sup> This structure is also believed to originate mainly from a region in the  $\Gamma$ - $X$ - $U$ - $L$  plane near  $\mathbf{k} = (2\pi/a)(\frac{3}{4}, \frac{1}{4}, \frac{1}{4})$ .<sup>49,105</sup> More recently, it is attributed to a small region centered at  $\mathbf{k} = (2\pi/a)(0.77, 0.29, 0.16)$ .<sup>106</sup> The  $\Delta_0$ ,  $\Delta'_0$ , and  $\Delta_1$  spin-orbit splittings of Ge are considerably larger than those of Si,<sup>103</sup> and thus the splitting-related transitions have been experimentally observed (see Table I).

### III. THEORETICAL EXPRESSION

The joint-density-of-states functions  $J_{cv}(\omega)$  can be related to the optical constant  $\epsilon_2(\omega)$  as follows:

$$\epsilon_2(\omega) = \frac{4\hbar^2 e^2}{\pi m^2 \omega^2} |\langle c | p | v \rangle|^2 J_{cv}(\omega), \quad (1)$$

where  $\langle |p| \rangle$  is the momentum matrix element for  $v$  (valence)  $\rightarrow c$  (conduction) transitions. In the following we try to obtain the model dielectric functions for the CP's of various transition energies ( $E_0$ ,  $E_0 + \Delta_0$ ,  $E_1$ ,  $E_1 + \Delta_1$ ,  $E_2$ ,  $E'_1$ , etc.). The effects of indirect-band-gap transitions which will take an important part in the analysis of the  $\epsilon_2$  spectrum (Si) are also discussed briefly.

#### A. $E_0$ and $E_0 + \Delta_0$ transitions

The  $E_0$  and  $E_0 + \Delta_0$  transitions in the diamond- and zinc-blende-type semiconductors occur in the center of the BZ ( $\Gamma$ ). These transitions are of the three-dimensional (3D)  $M_0$  CP's. Assuming the bands are parabolic, we obtain the contribution of these gaps to  $\epsilon_2(\omega)$  and  $\epsilon_1(\omega)$  (Ref. 107):

$$\begin{aligned} \epsilon_2(\omega) = & [A / (\hbar\omega)^2] [(\hbar\omega - E_0)^{0.5} H(\chi_0 - 1) \\ & + \frac{1}{2}(\hbar\omega - E_0 - \Delta_0)^{0.5} H(\chi_{s.o.} - 1)], \end{aligned} \quad (2)$$

$$\epsilon_1(\omega) = AE_0^{-1.5} [f(\chi_0) + \frac{1}{2} [E_0/(E_0 + \Delta_0)]^{1.5} f(\chi_{s.o.})], \quad (3)$$

with

$$A = \frac{4}{3} (\frac{3}{2} m^*)^{1.5} P^2, \quad (4)$$

$$f(\chi_0) = \chi_0^{-2} [2 - (1 + \chi_0)^{0.5} - (1 - \chi_0)^{0.5} H(1 - \chi_0)], \quad (5a)$$

$$f(\chi_{s.o.}) = \chi_{s.o.}^{-2} [2 - (1 + \chi_{s.o.})^{0.5} - (1 - \chi_{s.o.})^{0.5} H(1 - \chi_{s.o.})], \quad (5b)$$

$$\chi_0 = \hbar\omega / E_0, \quad (6a)$$

$$\chi_{s.o.} = \hbar\omega / (E_0 + \Delta_0), \quad (6b)$$

and

$$H(y) = \begin{cases} 1 & \text{for } y \geq 0 \\ 0 & \text{for } y < 0. \end{cases} \quad (7)$$

In Eq. (4),  $m^*$  is the combined density-of-states mass and  $P^2$  is the squared momentum matrix element.

As we will see later, the strength of the  $E_0$  and  $E_0 + \Delta_0$  transitions in Ge is very weak. This is due to the small density of states associated with these transitions (i.e., due to the small effective mass of the  $\Gamma_2'$  conduction band). However, we can clearly see the  $E_0/(E_0 + \Delta_0)$  structures in the optical spectrum of Ge in the region very close to the fundamental absorption edge.<sup>68-71,108</sup>

The  $E_0/(E_0 + \Delta_0)$  structures in Si, on the other hand, appear in spectrum between the dominant  $E_1$  and  $E_2$  structures.<sup>63,98</sup> As a result, its exceedingly weak nature would be completely covered with them. Because of this reason, we shall not take into account the contribution of these transitions in the  $\epsilon(\omega)$  spectra of Si.

### B. $E_1$ and $E_1 + \Delta_1$ transitions

Band-structure calculations and some experimental work indicated that the  $E_1$  and  $E_1 + \Delta_1$  transitions take place along the  $\langle 111 \rangle$  directions ( $\Lambda$ ) of the BZ. These CP's are of the 3D  $M_1$  type and occur in the region near 3.4 eV ( $E_1$ ) for Si and near 2.1 eV ( $E_1$ ) and 2.3 eV ( $E_1 + \Delta_1$ ) for Ge. The contributions to  $\epsilon_2(\omega)$  of this type are<sup>107</sup>

$$\epsilon_2(\omega) = \begin{cases} \pi\chi_1^{-2} [B_1 - B_{11}(E_1 - \hbar\omega)^{0.5}] & (\hbar\omega < E_1), \\ \pi B_1 \chi_1^{-2} & (\hbar\omega \geq E_1) \end{cases} \quad (8)$$

for the  $E_1$  transitions, and

$$\epsilon_2(\omega) = \begin{cases} \pi\chi_{1s}^{-2} [B_2 - B_{21}(E_1 + \Delta_1 - \hbar\omega)^{0.5}] & (\hbar\omega < E_1 + \Delta_1), \\ \pi B_2 \chi_{1s}^{-2} & (\hbar\omega \geq E_1 + \Delta_1) \end{cases} \quad (9)$$

for the  $E_1 + \Delta_1$  transitions, where

$$\chi_1 = \hbar\omega / E_1, \quad (10a)$$

$$\chi_{1s} = \hbar\omega / (E_1 + \Delta_1). \quad (10b)$$

In Eqs. (8) and (9), the  $B$ 's are the strength parameters. Since the  $M_1$  CP longitudinal effective mass is much

larger than its transverse counterparts, one can treat these 3D  $M_1$  CP's as two-dimensional (2D) minima  $M_0$ . The contribution to  $\epsilon_2(\omega)$  of this type of 2D minima is given by

$$\epsilon_2(\omega) = \pi [B_1 \chi_1^{-2} H(\chi_1 - 1) + B_2 \chi_{1s}^{-2} H(\chi_{1s} - 1)], \quad (11)$$

where the  $H$ 's are functions defined by Eq. (7).

The contribution of the  $E_1$  and  $E_1 + \Delta_1$  transitions to  $\epsilon_1(\omega)$  can be calculated from Eq. (11) by using the KK transformation. The result is

$$\epsilon_1(\omega) = -B_1 \chi_1^{-2} \ln(1 - \chi_1^2) - B_2 \chi_{1s}^{-2} \ln(1 - \chi_{1s}^2). \quad (12)$$

The first and second term on the right-hand side of Eq. (12), respectively, correspond to the  $E_1$ - and  $(E_1 + \Delta_1)$ -gap contributions.

### C. $E_2$ transitions

The  $E_2$  structure appears in the region near 4.3 eV for Si and near 4.4 eV for Ge. As mentioned in Sec. II, the nature of the  $E_2$  transitions is more complicated: it does not correspond to a single, well-defined CP. The structure in Si had been tried to be characterized by a one-dimensional (1D) maximum,<sup>109</sup> a mixture of a 2D  $M_1$  and a 2D  $M_2$ ,<sup>19</sup> or a mixture of a 3D  $M_1$  and a 3D  $M_2$  CP.<sup>63,91</sup> The  $E_2$  structure in Ge could be fitted using either a 3D  $M_2$  or a mixture of a 2D  $M_1$  and a 2D  $M_2$  CP.<sup>7</sup>

Here we shall characterize the  $E_2$  structure as that of a damped harmonic oscillator (DHO). This oscillator gives

$$\epsilon_2(\omega) = C\chi_2\gamma / [(1 - \chi_2^2)^2 + \chi_2^2\gamma^2], \quad (13)$$

$$\epsilon_1(\omega) = C(1 - \chi_2^2) / [(1 - \chi_2^2)^2 + \chi_2^2\gamma^2], \quad (14)$$

with

$$\chi_2 = \hbar\omega / E_2, \quad (15)$$

where  $C$  and  $\gamma$  are, respectively, the strength and damping parameters of the oscillator.

The DHO model provides a Lorentzian-like line shape (see Figs. 2 and 3), and in the limit  $\gamma \rightarrow 0$  the  $\epsilon_2$  spectrum exhibits a divergence at  $\hbar\omega = E_2$ . We can also regard the  $E_2$  gap as the CP of 2D  $M_1$  type. The contribution to  $\epsilon_2$  of this type is

$$\epsilon_2(\omega) = \pi\chi_2^{-2} (D_1 \ln |1 - \chi_2| - D_2), \quad (16)$$

where the  $D$ 's are the strength parameters. Equation (16) exhibits a divergence at  $\chi_2 = 1.0$  (i.e.,  $\hbar\omega = E_2$ ), and its spectrum very much resembles that of the DHO model when we take into account the damping effect in the equation. Therefore, we can say that the DHO is a different representation of the broadened 2D  $M_1$  CP. It is also interesting to point out<sup>110</sup> that variation of CP anisotropy parameters from three to two dimensions changes the density-of-states functions from  $M_1$  and  $M_2$  CP's (3D) to  $M_1$  (2D). This simply means that the 2D  $M_1$  CP originates from the 3D  $M_1$  and  $M_2$  CP's.

We found that the  $E_2$  structures in some III-V compounds (such as InSb, GaAs, GaP, and  $\text{Al}_x\text{Ga}_{1-x}\text{As}$ )

(Refs. 107 and 111) can be well fitted by the DHO model. However, unfortunately the structures in semiconductors of group IV (Si and Ge) are not reasonably fitted only by the DHO. We find that the best result is obtained with a mixture of the DHO and a 2D maxima ( $M_2$ ).

The contribution of the 2D  $M_2$  CP to  $\epsilon_2(\omega)$  is written as

$$\epsilon_2(\omega) = \begin{cases} \pi F \chi_2^{-2} (\hbar\omega \leq E_2), \\ 0 (\hbar\omega > E_2), \end{cases} \quad (17)$$

where  $F$  is the strength of the 2D  $M_2$  CP.

The conduction and valence bands reducing to infinitely small energies implied by Eq. (17) should be nonphysical. Because of this reason, we now modify the model by taking into account a low-energy cutoff at the energy  $E_{cl}$ . This modification provides

$$\epsilon_2(\omega) = \pi F \chi_2^{-2} H(\chi_{cl} - 1), \quad (18)$$

with

$$\chi_{cl} = \hbar\omega / E_{cl}. \quad (19)$$

The KK transformation of Eq. (18) gives

$$\epsilon_1(\omega) = -F \chi_2^{-2} \ln \left[ \frac{1 - \chi_{cl}^2}{1 - \chi_2^2} \right]. \quad (20)$$

In Figs. 2 and 3, respectively, we show the line shapes of the  $E_2$ -gap contribution to  $\epsilon(\omega)$  for Si and Ge. The dashed lines correspond to the DHO [ $\epsilon_2$ , Eq. (13);  $\epsilon_1$ , Eq. (14)], and the solid lines are the results of a mixture of the DHO and 2D  $M_2$  CP [ $\epsilon_2$ , Eq. (18);  $\epsilon_1$ , Eq. (20)]. The numerical parameters used in the calculations are listed in Table III. Here, the low-energy cutoff  $E_{cl}$  in Eqs. (18)–(20) is assumed to be the same value as  $E_1$  (i.e.,

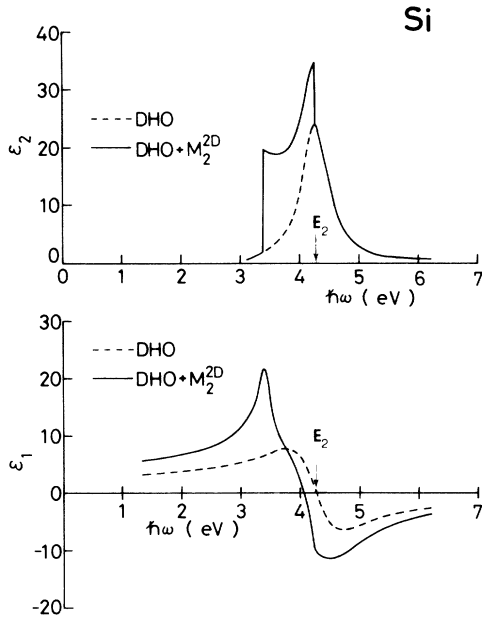


FIG. 2. Line shapes of the  $E_2$ -gap contribution to  $\epsilon(\omega)$  for Si. The dashed lines correspond to the DHO [ $\epsilon_2$ , Eq. (13);  $\epsilon_1$ , Eq. (14)]. The solid lines are the results of a mixture of the DHO and 2D  $M_2$  CP [ $\epsilon_2$ , Eq. (18);  $\epsilon_1$ , Eq. (20)].

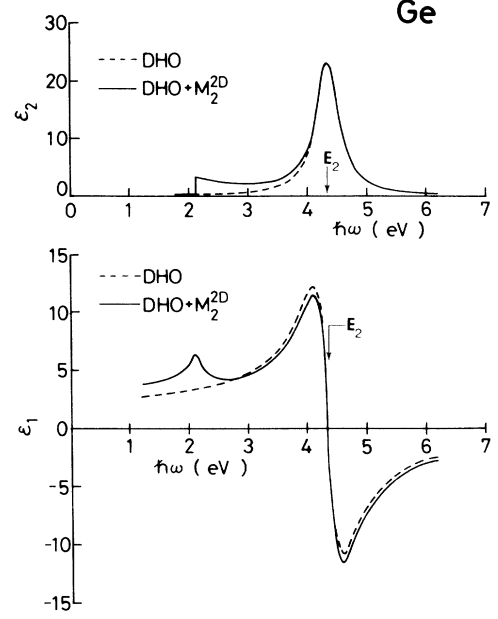


FIG. 3. Line shapes of the  $E_2$ -gap contribution to  $\epsilon(\omega)$  for Ge. The dashed lines correspond to the DHO [ $\epsilon_2$ , Eq. (13);  $\epsilon_1$ , Eq. (14)]. The solid lines are the results of a mixture of the DHO and 2D  $M_2$  CP [ $\epsilon_2$ , Eq. (18);  $\epsilon_1$ , Eq. (20)].

TABLE III. Parameters used in the calculation of  $\epsilon_1(\omega)$  and  $\epsilon_2(\omega)$ .

Parameter	Material	
	Si	Ge
$E_0$ (eV)		0.80
$E_0 + \Delta_0$ (eV)		1.09
$A$ (eV <sup>1.5</sup> )		2.70
$E_1$ (eV)	3.38	2.11
$E_1 + \Delta_1$ (eV)		2.30
$B_1$	5.22	3.79
$B_{11}$ (eV <sup>-0.5</sup> )	7.47	5.08
$B_2$		3.29
$B_{21}$ (eV <sup>-0.5</sup> )		7.35
$\Gamma[E_1/(E_1 + \Delta_1)]$ (eV)	0.05	0.07
$E_2$ (eV)	4.27	4.35
$C$	3.01	2.51
$\gamma$	0.127	0.109
$F$	3.51	0.23
$\Gamma(E_2)$ (eV)	0.04	0.04
$E_a$ (eV) <sup>a</sup>	5.32	5.80
$C_a$	0.21	0.51
$\gamma_a$	0.089	0.156
$E_b$ (eV) <sup>b</sup>		3.30
$C_b$		0.91
$\gamma_b$		0.140
$E_c$ (eV) <sup>b</sup>		3.80
$C_c$		1.33
$\gamma_c$		0.133
$E_g^{\text{td}}$ (eV)	1.12	
$D$	0.89	
$\epsilon_{1\infty}$	1.8	2.7

<sup>a</sup>This energy corresponds to the  $E'_1$  gap (see Tables I and II).

<sup>b</sup>These take account of the [ $E'_0$  (triplet)]-gap contribution.

$E_{cl}=E_1$ ). An addition of the 2D  $M_1$  component to the DHO one increases optical density ( $\epsilon_2$ ) in the low-energy region and produces a new structure in  $\epsilon_1$  in the region close to  $E_{cl}$ . As we will see in the next section, a considerably larger strength of the 2D  $M_2$  CP is required for Si to achieve a fit with experimental data.

#### D. $E'_1, E'_0, E'_0 + \Delta'_0$ , and $E'_0 + \Delta'_0 + \Delta_0$ transitions

The  $E'_1$  transitions are seen in optical spectra near 5.3 eV for Si and near 5.8 eV for Ge. Their structures could be characterized by the 2D  $M_1$  saddle point<sup>19</sup> or the 3D  $M_1$  (or  $M_2$ ) CP.<sup>63</sup> For Si the  $E'_0$  structure lies very close to the  $E_1$  region.<sup>59,60,63,64</sup> The  $E'_0$  triplet ( $E'_0, E'_0 + \Delta'_0$ , and  $E'_0 + \Delta'_0 + \Delta_0$ ) in Ge, on the other hand, appears in the energy region between the dominant  $E_1$  and  $E_2$  structures. They were treated either as a 2D  $M_0$  (room temperature) (Ref. 19) or a 3D  $M_0$  CP.<sup>60,63,64</sup>

In previous works,<sup>107,111,112</sup> no attention had been paid to the  $E'_1$  and  $E'_0$  (triplet) transitions in analyses of optical constants of semiconductors (GaSb, InAs, GaP, etc.). This is because they are too weak to be dominant in optical spectra.<sup>113</sup> For completeness, we shall take into account these transitions, but for simplicity we assume their nature to be as the following DHO's:<sup>114</sup>

$$\epsilon_2(\omega) = \sum_i C_i \chi_i \gamma_i / [(1 - \chi_i^2)^2 + \chi_i^2 \gamma_i^2], \quad (21)$$

$$\epsilon_1(\omega) = \sum_i C_i (1 - \chi_i^2) / [(1 - \chi_i^2)^2 + \chi_i^2 \gamma_i^2], \quad (22)$$

with

$$\chi_i = \hbar\omega / E_i, \quad (23)$$

where the  $E_i$ 's are the energies of corresponding oscillators.

#### E. Indirect-band-gap transitions

Si and Ge are indirect-band-gap semiconductors. The lowest indirect band gap of Si is  $\sim 1.1$  eV and that of Ge is  $\sim 0.8$  eV. The transition mechanism at the indirect band gap,  $E_g^{\text{id}}$ , is expressed by a second-order process in the perturbation. Using the result of the perturbation calculation, we can write the contribution of the indirect optical transitions to  $\epsilon_2(\omega)$  as

$$\epsilon_2(\omega) = \frac{G}{(\hbar\omega)^2} (\hbar\omega - E_g^{\text{id}} \pm \hbar\omega_q)^2 H(1 - \chi_g), \quad (24)$$

with

$$\chi_g = (E_g^{\text{id}} \pm \hbar\omega_q) / \hbar\omega, \quad (25)$$

where  $G$  is the direct-transition strength parameter,  $\hbar\omega_q$  is the phonon energy taking part in the indirect transitions, and  $H$  is a function defined by Eq. (7).

The parabolic bands extending to infinite energies implied by Eq. (24) should also be nonphysical. We shall, therefore, modify the model in a manner similar to that mentioned in Sec. III C by taking into account a high-energy cutoff at the energy  $E_{ch}$ . This modification gives

$$\epsilon_2(\omega) = \frac{G}{(\hbar\omega)^2} (\hbar\omega - E_g^{\text{id}} \pm \hbar\omega_q)^2 H(1 - \chi_g) H(1 - \chi_{ch}), \quad (26)$$

with

$$\chi_{ch} = \hbar\omega / E_{ch}. \quad (27)$$

Unfortunately, there has been no expression for the contribution of the indirect transitions to  $\epsilon_1(\omega)$ . Analytical expressions for this contribution from the KK transformation are also not yet available. We will, therefore, take into account the contribution of the indirect transitions only to  $\epsilon_2(\omega)$ , but not to  $\epsilon_1(\omega)$ .

## IV. RESULTS AND DISCUSSION

The models given in Sec. III can be used to fit the experimental dispersion of  $\epsilon_2$  and  $\epsilon_1$  over most of the spectral range (0–6.0 eV). The experimental data of  $\epsilon_1$  in the transparency region are, however, usually somewhat smaller than those of our model (i.e., the sum of each contribution). In order to improve a fit, therefore, we shall consider an additional term,  $\epsilon_{1\infty}$ , to  $\epsilon_1$ . This term is assumed to be nondispersive (i.e., constant).

### A. Silicon

The fits with our model to the experimental  $\epsilon_2$  of Si are shown in Fig. 4. The experimental data are taken from Aspnes and Studna (Ref. 4). The solid line is obtained from the sum of Eqs. (8) ( $E_1$  gap; 3D  $M_1$  CP), (13) ( $E_2$  gap; DHO), (18) ( $E_2$  gap; 2D  $M_2$  CP), (21) ( $E'_1$  gap; DHO), and (26) (indirect-band-gap transitions). The dashed line is from the sum of Eqs. (8), (13), (18), and (26) [i.e., without taking account of Eq. (21)]. The dotted line is the result of the sum of Eqs. (11) ( $E_1$  gap; 2D  $M_0$  CP), (13), (18), (21), and (26). We consider in Eq. (21) only one oscillator which corresponds to the  $E'_1$  transitions [i.e.,  $E_i (i=a) = E'_1$ ]. In Eq. (26) the high-energy cutoff  $E_{ch}$  is assumed to be  $E_{ch} = E_1$ . The numerical parameters of the fits used are listed in Table III.

The strength of the  $E_0/(E_0 + \Delta_0)$  transitions in Si is rather small,<sup>98</sup> and it can be seen to be successfully neglected here. It is also clear from the figure that the DHO model [Eq. (21)] interprets the  $E'_1$  structure ( $\sim 5.3$  eV) well. As discussed in Sec. III B, we are able to fit the  $E_1$  CP structure with either the 3D [Eq. (8); solid line] or 2D model [Eq. (11); dotted line]. The 3D model explains the experimental lower-energy shoulder of this structure well. The fit in the (1–2)-eV region also becomes satisfactory when the indirect-band-gap contribution [Eq. (26)] is taken into account.

Figure 5 shows the fits with our model to the experimental  $\epsilon_1$  spectrum of Si. The theoretical curves are obtained from the sum of Eqs. (12) ( $E_1$  gap; 2D  $M_0$  CP), (14) ( $E_2$  gap; DHO), (20) ( $E_2$  gap; 2D  $M_2$  CP), and (22) ( $E'_1$  gap; DHO). The nondispersive term,  $\epsilon_{1\infty}$  (=1.8), is also taken into consideration in this summation. The experimental data are taken below 1.5 eV from Philipp and Ehrenreich (Ref. 21; open circles) and those in the

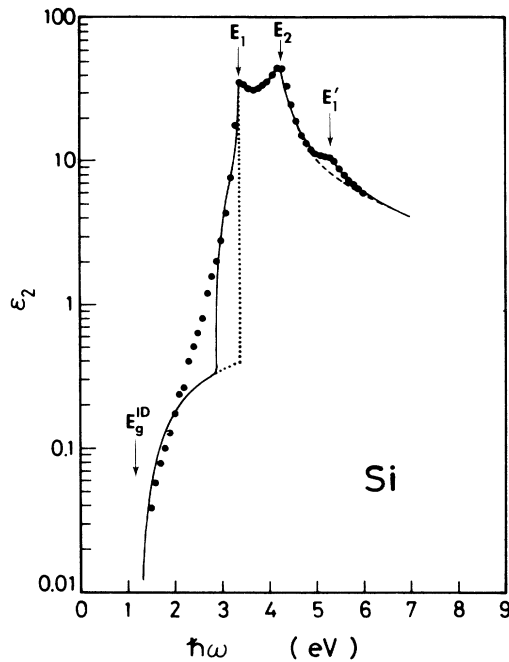


FIG. 4.  $\epsilon_2$  spectrum of Si. The solid line is obtained from the sum of Eqs. (8) ( $E_1$  gap; 3D  $M_1$  CP), (13) ( $E_2$  gap; DHO), (18) ( $E_2$  gap; 2D  $M_2$  CP), (21) ( $E'_1$  gap; DHO), and (26) (indirect-band-gap transitions). The dashed line is taken by the sum of Eqs. (8), (13), (18), and (26) [i.e., without taking account of Eq. (21)]. The dotted line is the result of the sum of Eqs. (11) ( $E_1$  gap; 2D  $M_0$  CP), (13), (18), (21), and (26). The experimental data are taken from Ref. 4 (solid circles).

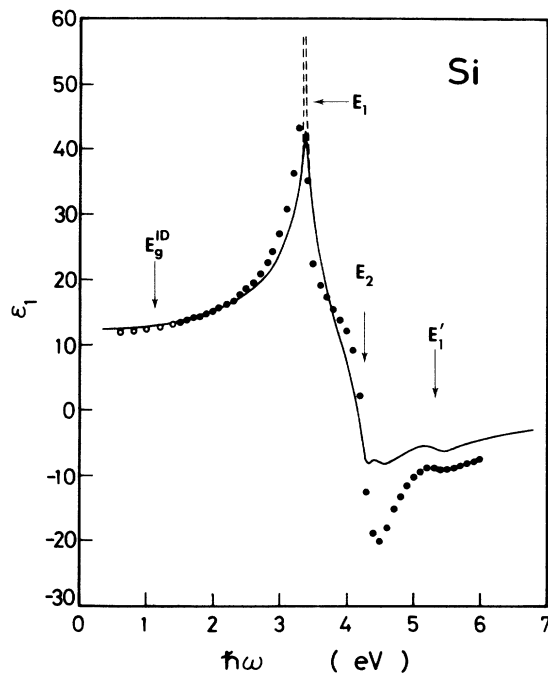


FIG. 5.  $\epsilon_1$  spectrum of Si. The theoretical curves are obtained from the sum of Eqs. (12) [ $E_1$  gap; 2D  $M_0$  CP,  $\Gamma=0$  eV (dashed line) and  $\Gamma=0.05$  eV (solid line)], (14) ( $E_2$  gap; DHO), (20) ( $E_2$  gap; 2D  $M_2$  CP), and (22) ( $E'_1$  gap; DHO). The non-dispersive term,  $\epsilon_{1\infty}$  ( $=1.8$ ), is also taken into consideration in this summation. The experimental data are taken from Refs. 21 (open circles) and 4 (solid circles).

(1.5–6.0)-eV range from Aspnes and Studna (Ref. 4; solid circles).

The theoretical  $\epsilon_1$  spectrum [Eq. (12)] exhibits a divergence at the  $E_1$  edge.<sup>107</sup> It is well known that the optical transitions are strongly affected by a damping effect (i.e., a lifetime broadening). The damping effect can be easily introduced in Eq. (12) in a phenomenological manner by replacing  $\omega$  by  $\omega + i(\Gamma/\hbar)$ . Variation of  $\epsilon_1(\omega)$  for a particular choice of the damping energy  $\Gamma$  is shown in Fig. 5 by the dashed ( $\Gamma=0$  eV) and solid lines ( $\Gamma=0.05$  eV). As seen in the figure, the damping effect can decrease the strength of the  $E_1$  structure and leads to a fact which is coincident with experimental verification. For the same reason, the value of  $\Gamma=0.04$  eV is also taken into consideration in the calculation of Eq. (20). It can be recognized that our model explains the  $\epsilon_1$  spectrum of Si well, especially in the energy region below 4 eV.

An individual contribution to  $\epsilon_2$  of the  $E_1$ ,  $E_2$ ,  $E'_1$ , and  $E_g^{\text{id}}$  transitions for Si is shown in Fig. 6. They are obtained from Eq. (8) for the  $E_1$ -gap contribution (3D  $M_1$  CP), from Eqs. (13) (DHO) and (18) (2D  $M_2$  CP) for the  $E_2$ -gap one, from Eq. (21) for the  $E'_1$ -gap one, and from Eq. (26) for the  $E_g^{\text{id}}$ -gap one. The sum of these contributions is shown by the bold line. The solid circles are the experimental data taken from Ref. 4.

The transitions at the  $E_g^{\text{id}}$  edge shown in Fig. 6 yield a continuous absorption spectrum characterized by a power law of  $(\hbar\omega)^{-2}(\hbar\omega - E_g^{\text{id}})^2$ . Because of the extremely low probability for indirect transitions, one can only expect to realize them experimentally below the direct threshold as a tail of the direct-absorption edge  $E_1$  (also see Fig. 4). The  $E_g^{\text{id}}$  transitions may also occur at energies above  $E_{ch}=E_1$ . However, the ensuing  $E_1$  and  $E_2$  transitions can provide sufficient strength and thus take

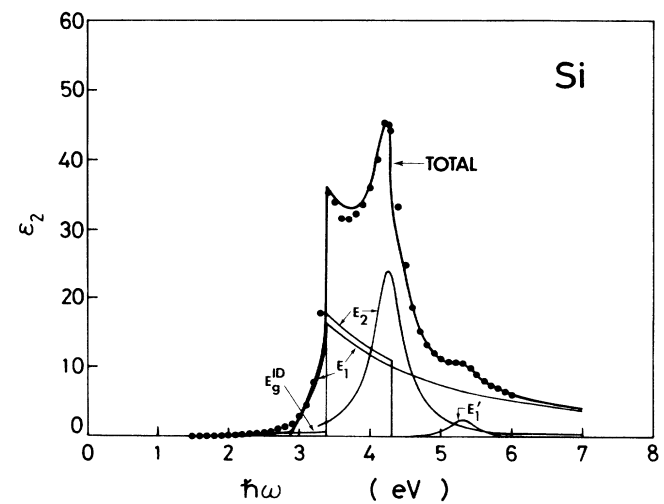


FIG. 6. Individual contribution to  $\epsilon_2$  of the  $E_1$ ,  $E_2$ ,  $E'_1$ , and  $E_g^{\text{id}}$  transitions for Si. They are obtained from Eq. (8) for the  $E_1$ -gap contributions (3D  $M_1$  CP), from Eqs. (13) (DHO) and (18) (2D  $M_2$  CP) for the  $E_2$ -gap one, from Eq. (21) for the  $E'_1$ -gap one, and from Eq. (26) for the  $E_g^{\text{id}}$ -gap one. The sum of these contributions is shown by the bold line. The solid circles are the experimental data taken from Ref. 4.

over the indirect-band-gap oscillators present at above  $E_{ch}$ .

The  $E_1$  gap is of the 3D  $M_1$  (or 2D  $M_0$ ) type. Hence, the line shape of the corresponding  $\epsilon_2$  spectrum should be characterized by a steep low-energy side and a broader high-energy side. This line shape is in good agreement with the experimental data. The strength parameter  $B_1$  can be given analytically by<sup>112</sup>

$$B_1 = \frac{32\sqrt{3}}{9\omega_1} \left[ \frac{a_B}{a_0} \right], \quad (28)$$

where  $a_B$  is the Bohr radius in Å,  $a_0$  the lattice constant in Å, and  $\omega_1$  the  $E_1$ -gap energy in hartrees (27.2 eV). Equation (28) predicts  $B_1=4.83$  at room temperature, while we obtained  $B_1=5.22$  from the present analysis. The agreement is extremely good in view of the crudeness of the theory used. A notable difference between the calculated and experimental values of  $B_1$  has, however, been found for InSb (Ref. 8) and GaP (Ref. 112), a fact that has been attributed to excitonic enhancement of the  $E_1$  transitions.<sup>75,115</sup> Some calculations<sup>63,116</sup> also showed that the  $k$ -linear term for  $k$  perpendicular to  $\langle 111 \rangle$  can significantly increase the strength of the  $E_1$  structure.

The  $E_2$  structure in Si can be fitted using a mixture of the DHO (broadened 2D  $M_1$  CP) and the 2D  $M_2$  CP. It is worth noting that the best-fit analyses of dielectric data in the  $E_2$ -structure region of group-(III-V) semiconductors required only the DHO contribution and no additional (2D  $M_2$  CP) one.<sup>107,111</sup> As is clearly seen in Fig. 6, the 2D  $M_2$  CP ( $E_2$  structure) has a considerably large strength. The steep low-energy end of this contribution at  $E_1$  is the result of the  $E_{cl}$  cutoff-energy modification. The strongest component in the  $\epsilon_2$  spectrum of Si is found to be the  $E_2$ -gap DHO. It is also recognized that the strength of the  $E'_1$  transitions is very weak.

### B. Germanium

A comparison of our  $\epsilon_2$  model to the experimental data of Ge is shown in Fig. 7. The experimental data are taken below 1.5 eV from Philipp and Ehrenreich (Ref. 21; open circles) and those in the (1.5–6.0)-eV range from Aspnes and Studna (Ref. 4; solid circles). The solid line is taken by the sum of Eqs. (2) [ $E_0/(E_0+\Delta_0)$  gaps; 3D  $M_0$  CP's], (8) ( $E_1$  gap; 3D  $M_1$  CP), (9) ( $E_1+\Delta_1$  gap; 3D  $M_1$  CP), (13) ( $E_2$  gap; DHO), (18) ( $E_2$  gap; 2D  $M_2$  CP), and (21) [ $E'_1, E'_0$  (triplet); DHO]. The dashed line is obtained from the sum of Eqs. (2), (8), (9), (13), and (18) [i.e., without taking account of Eq. (21)]. The dotted line is the result of the sum of Eqs. (2), (11) [ $E_1/(E_1+\Delta_1)$  gaps; 2D  $M_0$  CP's], (13), (18), and (21).

As in Si, the indirect transitions ( $E_g^{id}$ ) in Ge take part at below the onset of the direct-band-gap transitions which occurs at  $\sim 0.8$  eV ( $E_0$  gap). However, the energy separation between the  $E_g^{id}$  gap and the lowest direct band gap ( $E_0$ ) for Ge is very small ( $\sim 0.1$  eV; see Table II) compared to that for Si ( $\sim 2$  eV; Table I). We can, therefore, successfully neglect the  $E_g^{id}$ -gap contribution for the case of Ge. [The  $E_0/(E_0+\Delta_0)$ -gap contribution

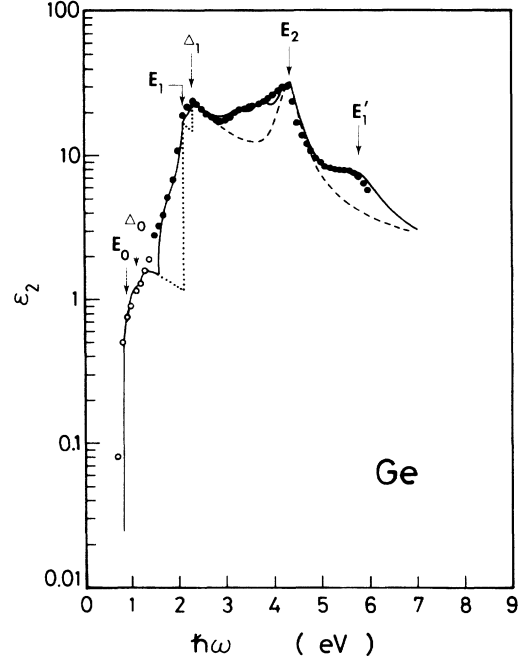


FIG. 7.  $\epsilon_2$  spectrum of Ge. The solid line is taken by the sum of Eqs. (2) [ $E_0/(E_0+\Delta_0)$  gaps; 3D  $M_0$  CP's], (8) ( $E_1$  gap; 3D  $M_1$  CP), (9) ( $E_1+\Delta_1$  gap; 3D  $M_1$  CP), (13) ( $E_2$  gap; DHO), (18) ( $E_2$  gap; 2D  $M_2$  CP), and (21) [ $E'_1, E'_0$  (triplet); DHO]. The dashed line is obtained from the sum of Eqs. (2), (8), (9), (13), and (18) [i.e., without taking account of Eq. (21)]. The dotted line is the result of the sum of Eqs. (2), (11) [ $E_1/(E_1+\Delta_1)$  gaps; 2D  $M_0$  CP's], (13), (18), and (21). The experimental data are taken from Refs. 21 (open circles) and 4 (solid circles).

can take over the weak  $E_g^{id}$ -gap one.] In fact, as shown in Fig. 7, we obtain a good fit with the experimental  $\epsilon_2$  spectrum in the fundamental absorption-edge region only by taking into account the  $E_0/(E_0+\Delta_0)$ -gap contribution [Eq. (2)].

We consider in Eq. (21) three DHO's: one corresponds to the  $E'_1$  transitions [ $E_i(i=a)=E'_1$ ] and the remaining two take into account the  $E'_0$  (triplet) transitions [ $E_i(i=b,c)$ ] (see Table III). A consideration of these components results in excellent agreement with the experimental  $\epsilon_2$  spectrum in the  $E'_1$ -edge region ( $\sim 5.8$  eV) and the region between 3 and 4.5 eV. The 3D  $M_1$  terms [Eqs. (8) and (9)] and a mixture of the DHO and 2D  $M_2$  terms [Eqs. (13) and (18)] also explain well the  $E_1/(E_1+\Delta_1)$  and  $E_2$  regions of the  $\epsilon_2$  spectrum, respectively. An excellent agreement can thus be achieved between our model (solid line) and the experimental data over a wide range of the photon energies.

The fits with our  $\epsilon_1$  model to the experimental data of Ge are shown in Fig. 8. The theoretical curves are obtained by the sum of Eqs. (3) [ $E_0/(E_0+\Delta_0)$  gaps; 3D  $M_0$ ], (12) [ $E_1/(E_1+\Delta_1)$  gaps; 2D  $M_0$ ], (14) ( $E_2$  gap; DHO), (20) ( $E_2$  gap; 2D  $M_2$ ), and (22) [ $E'_1, E'_0$  (triplet); DHO]. The nondispersive term,  $\epsilon_\infty$  ( $=2.7$ ), is also taken into consideration in this summation. The dashed line is obtained with  $\Gamma=0$  eV [Eq. (12)] and  $\Gamma=0.04$  eV [Eq. (20)], while the solid line is obtained with  $\Gamma=0.07$  eV

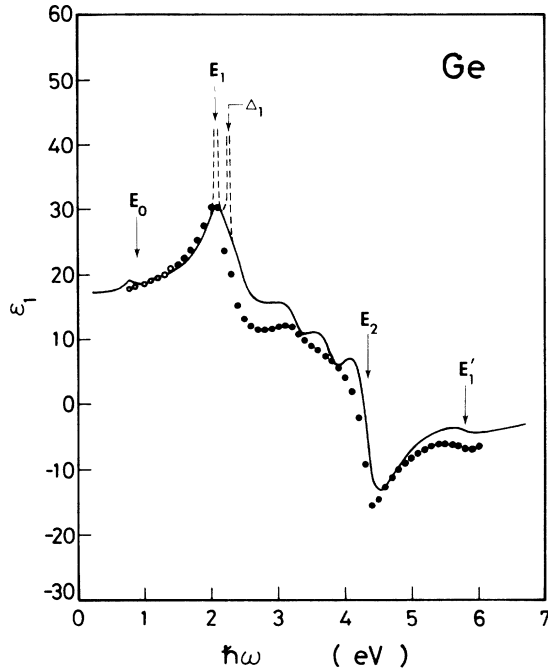


FIG. 8.  $\epsilon_1$  spectrum of Ge. The theoretical curves are obtained by the sum of Eqs. (3) [ $E_0/(E_0 + \Delta_0)$  gaps; 3D  $M_0$ ], (12) [ $E_1/(E_1 + \Delta_1)$  gaps; 2D  $M_0$ ,  $\Gamma = 0$  eV (dashed line) and  $\Gamma = 0.07$  eV (solid line)] (14) ( $E_2$  gap; DHO), (20) ( $E_2$  gap; 2D  $M_2$ ), and (22) [ $E'_1$ ,  $E'_0$  (triplet); DHO]. The nondispersive term,  $\epsilon_\infty$  ( $= 2.7$ ), is also taken into consideration in this summation. The experimental data are taken from Refs. 21 (open circles) and 4 (solid circles).

[Eq. (12)] and  $\Gamma = 0.04$  eV [Eq. (20)]. The experimental data are taken from Refs. 21 (open circles) and 4 (solid circles).

As discussed before, the smaller the damping energy in Eq. (12) gives the larger the  $E_1$ -peak value. The experimental value of  $\epsilon_1$  at the  $E_1$  peak is 30.1. Calculation of Eq. (12) with  $\Gamma = 0.07$  eV (solid line) agrees well with this peak value. Equations (14) and (20) also interpret the peculiar line shape of the  $E_2$  structure well [see (4–6)-eV spectrum region in Fig. 8].

An individual contribution to  $\epsilon_2$  of the  $E_0/(E_0 + \Delta_0)$ ,  $E_1/(E_1 + \Delta_1)$ ,  $E_2$ ,  $E'_1$ , and  $E'_0$  (triplet) gaps for Ge is shown in Fig. 9. They are obtained from Eq. (2) for the  $E_0/(E_0 + \Delta_0)$ -gap contribution (3D  $M_0$  CP), from Eq. (8) for the  $E_1$ -gap one (3D  $M_1$  CP), from Eq. (9) for the  $(E_1 + \Delta_1)$ -gap one (3D  $M_1$  CP), from Eqs. (13) (DHO) and (17) (2D  $M_2$  CP) for the  $E_2$ -gap one, from Eq. (21) for the  $E'_1$ -gap (DHO) and [ $E'_0$  (triplet)]-gap ones [DHO; marked in the figure by  $(E'_0/\Delta'_0/\Delta_0)$ ]. The bold line in the figure is the sum of these contributions. The open and solid circles are the experimental data taken from Refs. 21 and 4, respectively.

The  $E_0/(E_0 + \Delta_0)$  transitions yield a continuous  $\epsilon_2(\omega)$  spectrum obeying the well-known  $\frac{1}{2}$  power law [i.e.,  $\propto (\hbar\omega)^{-2}(\hbar\omega - E_0)^{0.5}$ ]. The transitions contribute strongly to the dispersion of  $\epsilon_1(\omega)$  but not to its absolute value.<sup>107,117,118</sup>

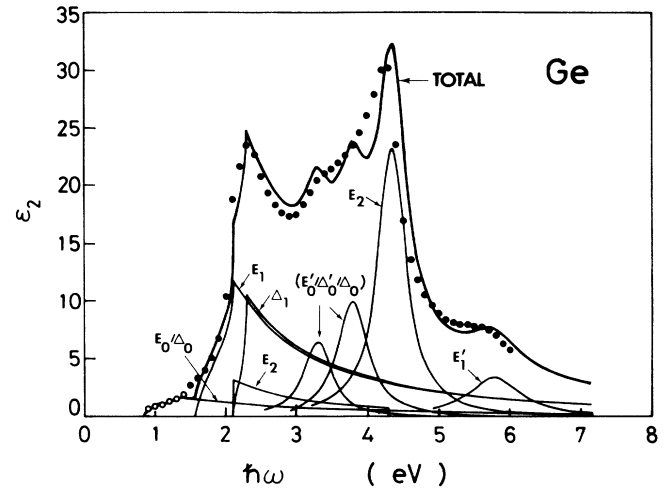


FIG. 9. Individual contribution to  $\epsilon_2$  of the  $E_0/(E_0 + \Delta_0)$ ,  $E_1/(E_1 + \Delta_1)$ ,  $E_2$ ,  $E'_1$ , and  $E'_0$  (triplet) gaps for Ge. They are obtained from Eq. (2) for the [ $E_0/(E_0 + \Delta_0)$ ]-gap contribution (3D  $M_0$  CP), from Eq. (8) for the  $E_1$ -gap one (3D  $M_1$  CP), from Eq. (9) for the  $(E_1 + \Delta_1)$ -gap one (3D  $M_1$  CP), from Eqs. (13) (DHO) and (17) (2D  $M_2$  CP) for the  $E_2$ -gap one, and from Eq. (21) for the  $E'_1$ -gap (DHO) and [ $E'_0$  (triplet)]-gap ones [DHO; marked by  $(E'_0/\Delta'_0/\Delta_0)$ ]. The bold line in the figure is the sum of these contributions. The open and solid circles are the experimental data taken from Refs. 21 and 4, respectively.

The strength of the  $E_1$  and  $E_1 + \Delta_1$  transitions of diamond (zinc-blende) materials can be estimated with the simple expression<sup>7-9,16,18,19</sup>

$$B_1 = 44 \frac{E_1 + \Delta_1/3}{a_0 E_1^2}, \quad (29a)$$

$$B_2 = 44 \frac{E_1 + 2\Delta_1/3}{a_0 (E_1 + \Delta_1)^2}, \quad (29b)$$

where  $a_0$  is the lattice constant in Å and  $E_1$  and  $\Delta_1$  are in eV. This expression predicts  $B_1 = 3.79$  and  $B_2 = 3.29$ . These values are used in the calculations of Eqs. (8)–(12). [The additional strength parameters  $B_{11}$  and  $B_{21}$  in Eqs. (8) and (9) are then determined from the best-fit procedures with the experimental  $\epsilon_2$  data (see Table III).] We can obtain good fits to the experimental  $\epsilon_1$  and  $\epsilon_2$  spectra using these predicted  $B_1$  and  $B_2$  values (Figs. 7 and 8).

The strength of the 2D  $M_2$  ( $E_2$ -gap) contribution for Ge is very weak, compared to that for Si (see Figs. 6 and 9). As mentioned in Sec. II, the energy-band structure of Ge has a stronger resemblance to those of zinc-blende, III–V materials (such as GaAs and InAs) rather than to that of Si. The best-fit analyses of dielectric data in the  $E_2$ -structure region of such III–V semiconductors required no or negligibly small 2D  $M_2$  contribution. A negligibly small or a weak strength of this contribution for Ge and some III–V semiconductors may come from their energy-band structures.

## V. CONCLUSIONS

We have developed a method for calculation of the real ( $\epsilon_1$ ) and imaginary parts ( $\epsilon_2$ ) of the dielectric function of Si and Ge at energies below and above the fundamental absorption edge. This model is based on the Kramers-Kronig transformation and takes into account the effects of interband transitions at the  $E_0$ ,  $E_0 + \Delta_0$ ,  $E_1$ ,  $E_1 + \Delta_1$ ,  $E_2$ ,  $E'_1$ , and  $E'_0$  (triplet) CP's and indirect band gaps. The  $E_0/(E_0 + \Delta_0)$  structures could be characterized by a 3D  $M_0$  CP, the  $E_1/(E_1 + \Delta_1)$  structures by a 3D  $M_1$  (or 2D  $M_0$ ) CP, the  $E_2$  structure by a mixture of damped harmonic oscillator (DHO; a broadened 2D  $M_1$  CP) and 2D  $M_2$  CP, and the  $E'_1$  and  $E'_0$  (triplet) structures by the DHO's. The indirect transitions are assumed to provide a gradually increasing absorption spectrum expressed by a power law of  $(\hbar\omega - E_g^{\text{id}})^2$  ( $\hbar\omega$  is the photon energy,  $E_g^{\text{id}}$  the indirect band gap). Analyses are presented for these semiconductors, and results are in satisfactory agreement

with the experimental data over the entire range of photon energies (0–6.0 eV). Line-shape analyses of  $\epsilon_1$  and  $\epsilon_2$  spectra yield information about the strength and broadening parameters of each CP. Dielectric-related optical constants, such as the refractive indices and the absorption coefficients, are easy to obtain from the present study in the form of practical functions. Since these expressions are purely analytical functions of the electronic energy-band parameters, the model would also be applicable to the analysis of some perturbation-induced effects of the optical constant (e.g., the pressure and temperature dependence of the refractive indices).

## ACKNOWLEDGMENT

This work was supported in part by the Gunma University Foundation for Science and Technology, Gunma, Japan.

- <sup>1</sup>J. Friedel, G. Harbeke, F. Abeles, B. O. Seraphin, J. Tauc, V. M. Granovich, J. G. Mavroides, M. Balkanski, H. Pick, W. E. Spicer, J. Ducuing, and C. Flytzanis, in *Optical Properties of Solids*, edited by F. Abeles (North-Holland, Amsterdam, 1972).
- <sup>2</sup>D. E. Aspnes, in *Optical Properties of Solids: New Developments*, edited by B. O. Seraphin (North-Holland, Amsterdam, 1976).
- <sup>3</sup>S. M. Kelso, D. E. Aspnes, M. A. Pollack, and R. E. Nahory, *Phys. Rev. B* **26**, 6669 (1982).
- <sup>4</sup>D. E. Aspnes and A. A. Studona, *Phys. Rev. B* **27**, 985 (1983).
- <sup>5</sup>L. Viña and M. Cardona, *Phys. Rev. B* **29**, 6739 (1984).
- <sup>6</sup>L. Viña, C. Umbach, M. Cardona, and L. Vodopyanov, *Phys. Rev. B* **29**, 6752 (1984).
- <sup>7</sup>L. Viña, S. Logothetidis, and M. Cardona, *Phys. Rev. B* **30**, 1979 (1984).
- <sup>8</sup>S. Logothetidis, L. Viña, and M. Cardona, *Phys. Rev. B* **31**, 947 (1985).
- <sup>9</sup>L. Viña, H. Höchst, and M. Cardona, *Phys. Rev. B* **31**, 958 (1985).
- <sup>10</sup>S. Logothetidis, P. Lautenschlager, and M. Cardona, *Phys. Rev. B* **33**, 1110 (1986).
- <sup>11</sup>M. Erman, J. P. Andre, and J. LeBris, *J. Appl. Phys.* **59**, 2019 (1986).
- <sup>12</sup>D. E. Aspnes, S. M. Kelso, R. A. Logan, and R. Bhat, *J. Appl. Phys.* **60**, 754 (1986).
- <sup>13</sup>S. Logothetidis, M. Cardona, P. Lautenschlager, and M. Garriga, *Phys. Rev. B* **34**, 2458 (1986).
- <sup>14</sup>B. Drevillon, E. Bertran, P. Alnot, J. Olivier, and M. Razeghi, *J. Appl. Phys.* **60**, 3512 (1986).
- <sup>15</sup>L. Viña and M. Cardona, *Phys. Rev. B* **34**, 2586 (1986).
- <sup>16</sup>P. Lautenschlager, M. Garriga, S. Logothetidis, and M. Cardona, *Phys. Rev. B* **35**, 9174 (1987).
- <sup>17</sup>M. Garriga, P. Lautenschlager, M. Cardona, and K. Ploog, *Solid State Commun.* **61**, 157 (1987).
- <sup>18</sup>P. Lautenschlager, M. Garriga, and M. Cardona, *Phys. Rev. B* **36**, 4813 (1987).
- <sup>19</sup>P. Lautenschlager, M. Garriga, L. Viña, and M. Cardona, *Phys. Rev. B* **36**, 4821 (1987).
- <sup>20</sup>S. Logothetidis and H. M. Polatoglou, *Phys. Rev. B* **36**, 7491 (1987).
- <sup>21</sup>H. R. Philipp and H. J. Ehrenreich, *Phys. Rev.* **129**, 1550 (1963).
- <sup>22</sup>D. K. Holmes, *Phys. Rev.* **66**, 326 (1944).
- <sup>23</sup>F. Herman and J. Callaway, *Phys. Rev.* **89**, 518 (1952).
- <sup>24</sup>T. O. Woodruff, *Phys. Rev.* **103**, 1159 (1956).
- <sup>25</sup>F. Bassani, *Phys. Rev.* **108**, 263 (1957).
- <sup>26</sup>J. C. Phillips, *Phys. Rev.* **112**, 685 (1958).
- <sup>27</sup>F. Herman, *Phys. Rev.* **93**, 1214 (1959).
- <sup>28</sup>L. Kleinman and J. C. Phillips, *Phys. Rev.* **118**, 1153 (1960).
- <sup>29</sup>D. Brust, M. L. Cohen, and J. C. Phillips, *Phys. Rev. Lett.* **9**, 94 (1962); **9**, 389 (1962).
- <sup>30</sup>F. Bassani and D. Brust, *Phys. Rev.* **131**, 1524 (1963).
- <sup>31</sup>D. Brust, *Phys. Rev.* **134**, A1337 (1964); **139**, A489 (1965).
- <sup>32</sup>M. L. Cohen and T. K. Bergstresser, *Phys. Rev.* **141**, 789 (1966).
- <sup>33</sup>M. Cardona and F. H. Pollak, *Phys. Rev.* **142**, 530 (1966).
- <sup>34</sup>E. O. Kane, *Phys. Rev.* **146**, 558 (1966).
- <sup>35</sup>F. Herman, R. L. Kortum, C. D. Kuglin, and R. A. Short, in *Quantum Theory of Atoms, Molecules, and the Solid State*, edited by P. O. Löwdin (Academic, New York, 1966).
- <sup>36</sup>W. Brinkman and B. Goodman, *Phys. Rev.* **149**, 597 (1966).
- <sup>37</sup>G. Dresselhaus and M. S. Dresselhaus, *Phys. Rev.* **160**, 649 (1967).
- <sup>38</sup>F. Herman, R. L. Kortum, C. D. Kuglin, J. P. van Dyke, and S. Skillman, in *Methods in Computing Physics*, edited by B. Alder, S. Fernbach, and M. Rotenberg (Academic, New York, 1968), Vol. 8.
- <sup>39</sup>L. R. Saravia and D. Brust, *Phys. Rev.* **171**, 916 (1968); **176**, 915 (1968); **178**, 1240 (1969).
- <sup>40</sup>D. Brust and E. O. Kane, *Phys. Rev.* **176**, 894 (1968).
- <sup>41</sup>D. J. Stukel and R. N. Euwema, *Phys. Rev. B* **1**, 1635 (1970).
- <sup>42</sup>A. K. Hochberg and C. R. Westgate, *J. Phys. Chem. Solids* **31**, 2317 (1970).
- <sup>43</sup>A. R. Williams, *Phys. Rev. B* **1**, 3417 (1970).
- <sup>44</sup>F. Beleznyay, *J. Phys. C* **3**, 1884 (1970).
- <sup>45</sup>R. C. Chaney, C. C. Lin, and E. E. Lafon, *Phys. Rev. B* **3**, 459 (1971).

- <sup>46</sup>H. Fock, *Phys. Status Solidi B* **56**, 463 (1973).
- <sup>47</sup>J. A. Appelbaum and D. R. Hamann, *Phys. Rev. B* **8**, 1777 (1973).
- <sup>48</sup>L. R. Saravia, *J. Phys. Chem. Solids* **35**, 1469 (1974).
- <sup>49</sup>J. R. Chelikowsky and M. L. Cohen, *Phys. Rev. Lett.* **31**, 1582 (1973); *Phys. Rev. B* **10**, 5095 (1974).
- <sup>50</sup>K. C. Pandey and J. C. Phillips, *Phys. Rev. B* **13**, 750 (1975).
- <sup>51</sup>E. O. Kane, *Phys. Rev. B* **13**, 3478 (1975).
- <sup>52</sup>J. R. Chelikowsky and M. L. Cohen, *Phys. Rev. B* **14**, 556 (1976).
- <sup>53</sup>L. Pasemann, *Phys. Status Solidi B* **84**, 175 (1977).
- <sup>54</sup>S. Ciraci and I. P. Batra, *Phys. Rev. B* **15**, 4923 (1977).
- <sup>55</sup>S. Antoci and L. Mihich, *Phys. Rev. B* **17**, 1859 (1978).
- <sup>56</sup>C. Tejedor and J. A. Vergés, *Phys. Rev. B* **19**, 2283 (1979).
- <sup>57</sup>A. Frova, P. Handler, F. A. Germano, and D. E. Aspnes, *Phys. Rev.* **145**, 575 (1966).
- <sup>58</sup>W. Bludau, A. Onton, and W. Heinke, *J. Appl. Phys.* **45**, 1846 (1974).
- <sup>59</sup>J. W. Grover and P. Handler, *Phys. Rev. B* **9**, 2600 (1974).
- <sup>60</sup>K. Kondo and A. Moritani, *Phys. Rev. B* **14**, 1577 (1976).
- <sup>61</sup>R. Zallen and W. Paul, *Phys. Rev.* **155**, 703 (1967).
- <sup>62</sup>M. Cardona, K. L. Shaklee, and F. H. Pollak, *Phys. Rev.* **154**, 696 (1967).
- <sup>63</sup>A. Daunois and D. E. Aspnes, *Phys. Rev. B* **18**, 1824 (1978).
- <sup>64</sup>G. Jungk, *Phys. Status Solidi B* **99**, 643 (1980).
- <sup>65</sup>E. Ehrenreich, H. R. Philipp, and J. C. Phillips, *Phys. Rev. Lett.* **8**, 59 (1962).
- <sup>66</sup>M. Cardona and D. L. Greenaway, *Phys. Rev.* **125**, 1291 (1962).
- <sup>67</sup>J. Humlíček, F. Lukeš, E. Schmidt, M. G. Kekoua, and E. Khoutsishvili, *Solid State Commun.* **47**, 387 (1983).
- <sup>68</sup>Y. Hamakawa, F. A. Germano, and P. Handler, *Phys. Rev.* **167**, 703 (1968).
- <sup>69</sup>B. O. Seraphin, R. B. Hess, and N. Bottka, *J. Appl. Phys.* **36**, 2242 (1965).
- <sup>70</sup>R. F. Potter, *Phys. Rev.* **150**, 562 (1966).
- <sup>71</sup>T. Nishino and Y. Hamakawa, *J. Phys. Soc. Jpn.* **26**, 403 (1969).
- <sup>72</sup>S. Koeppen, P. Handler, and S. Jaspersen, *Phys. Rev. Lett.* **27**, 265 (1971).
- <sup>73</sup>T. Takizawa, H. Fukutani, and G. Kuwabara, *J. Phys. Soc. Jpn.* **35**, 543 (1973).
- <sup>74</sup>D. E. Aspnes and J. E. Rowe, *Phys. Rev. B* **7**, 887 (1973).
- <sup>75</sup>J. Humlíček, *Phys. Status Solidi B* **86**, 303 (1978).
- <sup>76</sup>K. L. Shaklee, F. H. Pollak, and M. Cardona, *Phys. Rev. Lett.* **15**, 883 (1965).
- <sup>77</sup>A. K. Ghosh, *Phys. Rev.* **165**, 888 (1968).
- <sup>78</sup>M. Cardona and G. Harbeke, *J. Appl. Phys.* **34**, 813 (1963).
- <sup>79</sup>T. M. Donovan, J. E. Fischer, J. Matsuzaki, and W. E. Spicer, *Phys. Rev. B* **3**, 4292 (1971).
- <sup>80</sup>D. E. Aspnes, *Phys. Rev. Lett.* **28**, 913 (1972).
- <sup>81</sup>R. R. L. Zucca and Y. R. Shen, *Phys. Rev. B* **1**, 2668 (1970).
- <sup>82</sup>G. E. Jellison, Jr. and F. A. Modine, *Phys. Rev. B* **27**, 7466 (1983).
- <sup>83</sup>E. Matatagui, A. G. Thompson, and M. Cardona, *Phys. Rev.* **176**, 950 (1968).
- <sup>84</sup>M. Welkowsky and R. Braunstein, *Phys. Rev. B* **5**, 497 (1972).
- <sup>85</sup>J. R. Chelikowsky and M. L. Cohen, *Phys. Rev. B* **14**, 556 (1976).
- <sup>86</sup>S. O. Sari and S. E. Schnatterly, *Surf. Sci.* **37**, 328 (1973).
- <sup>87</sup>J. Koo, Y. R. Shen, and R. R. L. Zucca, *Solid State Commun.* **9**, 2229 (1971).
- <sup>88</sup>G. S. Wepfer, T. C. Collins, and R. N. Euwema, *Phys. Rev. B* **4**, 1296 (1971).
- <sup>89</sup>D. J. Chadi, *Phys. Rev. B* **16**, 790 (1977).
- <sup>90</sup>F. H. Pollak, *Surf. Sci.* **37**, 863 (1973).
- <sup>91</sup>K. Kondo and A. Moritani, *Phys. Rev. B* **15**, 812 (1977).
- <sup>92</sup>G. Guizzetti, L. Nosenzo, E. Reguzzoni, and G. Samoggia, *Phys. Rev. B* **9**, 640 (1974).
- <sup>93</sup>F. R. Kessler and K. Dettmer, *Phys. Status Solidi B* **51**, 79 (1972).
- <sup>94</sup>D. E. Aspnes, *Phys. Rev. Lett.* **31**, 230 (1973).
- <sup>95</sup>H. R. Philipp and E. A. Taft, *Phys. Rev.* **113**, 1002 (1959); **120**, 37 (1960).
- <sup>96</sup>I. Balslev, *Solid State Commun.* **5**, 315 (1967).
- <sup>97</sup>J. E. Fischer and N. Bottka, *Phys. Rev. Lett.* **24**, 1292 (1970).
- <sup>98</sup>D. E. Aspnes and A. A. Studna, *Solid State Commun.* **11**, 1375 (1972).
- <sup>99</sup>D. D. Sell and E. O. Kane, *Phys. Rev. B* **5**, 417 (1972).
- <sup>100</sup>W. Paul, *J. Appl. Phys. (Suppl.)* **32**, 2082 (1961).
- <sup>101</sup>A. Gavini and M. Cardona, *Phys. Rev. B* **1**, 672 (1970).
- <sup>102</sup>G. Guizzetti, L. Nosenzo, E. Reguzzoni, and G. Samoggia, *Phys. Rev. B* **9**, 640 (1974).
- <sup>103</sup>J. S. Kline, F. H. Pollak, and M. Cardona, *Helv. Phys. Acta* **41**, 968 (1968).
- <sup>104</sup>H. Jones, *The Theory of Brillouin Zones and Electronic States in Crystals* (North-Holland, Amsterdam, 1960).
- <sup>105</sup>C. W. Higginbotham, F. H. Pollak, and M. Cardona, *Solid State Commun.* **5**, 513 (1967).
- <sup>106</sup>W. D. Grobman, D. E. Eastman, and J. L. Freeouf, *Phys. Rev. B* **12**, 4405 (1975).
- <sup>107</sup>S. Adachi, *Phys. Rev. B* **35**, 7454 (1987).
- <sup>108</sup>M. V. Hobden, *J. Phys. Chem. Solids* **23**, 821 (1962).
- <sup>109</sup>L. Viña, C. Umbach, A. Compaan, M. Cardona, and A. Axmann, *J. Phys. (Paris) Colloq.* **44**, C5-203 (1983).
- <sup>110</sup>Y. Hamakawa and T. Nishino, in *Optical Properties of Solids: New Developments*, edited by B. O. Seraphin (North-Holland, Amsterdam, 1976).
- <sup>111</sup>S. Adachi, *Phys. Rev. B* **38**, 12 345 (1988).
- <sup>112</sup>K. Strössner, S. Ves, and M. Cardona, *Phys. Rev. B* **32**, 6614 (1985).
- <sup>113</sup>The band-structure calculation of Chelikowsky and Cohen (Ref. 52) for InP suggests four CP's in the (4.5–5.5)-eV energy region. Two of them correspond to transitions at the  $\Gamma$  point [ $\Gamma_8^+ \rightarrow \Gamma_7^-$  at 4.64 eV and  $\Gamma_8^+ \rightarrow \Gamma_8^+$  at 5.13 eV (Ref. 18)], and they are labeled  $E'_0$  and  $E'_0 + \Delta'_0$ . In earlier work (Ref. 62), these transitions were attributed to an  $E_2$  CP. The  $E_2$  transitions occur in the region near the  $E'_0$  and  $E'_0 + \Delta'_0$  CP's, but their strength is weaker than that of the  $E'_0$  and  $E'_0 + \Delta'_0$  transitions. Thus, it is worth noting that in InP the strength of the  $E'_0$  and  $E'_0 + \Delta'_0$  transitions is relatively strong and dominant enough in optical spectra (see, e.g., Ref. 18).
- <sup>114</sup>The  $E'_0$  (triplet) CP's would have a 3D  $M_0$  character. We also treated their structures in Ge as the 3D  $M_0$  type [i.e., Eqs. (2) and (3)]. However, this treatment led to a poorer fit with the experimental data than that using the DHO. This fact may be due to the multitude of possible CP's in the  $E'_0$  spectral region, which may give rise to an averaging over several CP's.
- <sup>115</sup>N. Meskini, W. Hanke, H. J. Mattausch, M. Balkanski, and M. Zouaghi, *J. Phys. (Paris)* **45**, 1707 (1984).
- <sup>116</sup>M. Cardona, *Phys. Rev. B* **15**, 5999 (1977).
- <sup>117</sup>M. A. Afromowitz, *Solid State Commun.* **15**, 59 (1974).
- <sup>118</sup>S. Adachi, *J. Appl. Phys.* **53**, 5863 (1982); **61**, 4869 (1987).